The 5th Joint International Conference on Multibody System Dynamics
June 24 – 28, 2018, Lisboa, Portugal

A transient EHL contact model capturing system-level spur gears dynamic behavior

Leoluca Scurria[1,2], Tommaso Tamarozzi[1,3], Pavel Jiránek[1] and Dieter Fauconnier[2,4]

[1]*Siemens Industry Software NV, Leuven, Belgium, leoluca.scurria@siemens.com, tommaso.tamarozzi@siemens.com*
[2]*Soete Laboratory, EEMMeCS, Gent University, Belgium*
[3]*KU Leuven, Leuven, Belgium*
[4]*Motion Products, Flanders Make*

ABSTRACT *The paper presents a strategy to model the transient behavior of spur gears accounting for EHL contacts by means of analytic fomulation. The contact modeling technique is then integrated with an FE-based approach to model the compliance of the gear bodies. The methodology is implemented in the Siemens PLM multibody Motion solver and the results are compared against experimental test data acquired on a back-to-back test-rig.*

1 Introduction

Mechanical transmissions are responsible for significant noise generation and power losses in automotive and wind energy applications. New regulations on pollution in terms of noises and the ever increasing demands for improved energy efficiency and increased power density are pushing the developments in gearboxes to lighter, more efficient and more silent designs. On the other hand, little is known about loss mechanisms and their effect on other crucial performance attributes such as noise and durability. A solution lies in the development and improvement of computational tools that predict the drivetrain system-level dynamics. One of the basic components of a transmission system are gears. In the vast majority of the cases, vibrations in a single rotating gear turn out to be above the audible hearing range (20 Hz to 20 KHz) which makes its dynamic response negligible with respect to NVH (Noise Vibration Harshness) analysis. However, when two or more gears are meshing, they excite each other and the surrounding structure with a frequency that depends on the time variation of the meshing conditions. This phenomenon usually happens at a substantially lower frequency within the audible range. The vibrational behavior of a geared transmission mostly depends on three characteristics: mass distribution, stiffness and damping.

In most of the cases, gears work in lubricated conditions, mainly to reduce friction and wear, provide cooling and remove debris and additionally provide damping and attenuate noise and vibrations. Indeed, for lubricated curved surfaces in relative motion with respect to each other, the lubricant is dragged by shear in the convergent gap, separating as such both surfaces due to increased hydrodynamic pressure. Because of the non-conformity of the contact between gears, the local pressure may rise up to the order of $1-5$ GPa, resulting into a significant elastic deformation of the opposing surfaces. Moreover, at such high pressures, the liquid lubricant becomes compressible and its viscosity rises locally (i.e. piezo-viscosity), resulting in a local solidification of the lubricant. Hence, this type of lubrication regime is denoted as elasto-hydrodynamic lubrication (EHL).

As pointed out by Andersson [1], when contacting gear teeth are loaded, the linear part of the displacement can be separated from the non-linear contact displacement. In this research, the linear load-deflection part is determined by an FE-based approach [2, 3, 4] which is capable of capturing phenomena such as the deformation of the gear body (fundamental in e.g. lightweight gears) and the global deformation of the teeth (e.g. tooth bending) assuming quasi-static loading conditions. The non-linear contact damping and stiffness are considered and determining them is the scope of the presented research. In general, EHL contacts represent a complex multiphysics problem, due to the two-way coupled interaction of the fluid film and the solid deformation. EHL contacts are

typically studied with either Reynolds equation in combination with Hertzian contact theory [5], or more recently, by advanced Computational Fluid Dynamics (CFD) and Fluid-Structure-Interaction [6] software. Both turn out to be prohibitively expensive to be employed in a multibody simulation environment. Therefore, throughout the last decade, the multibody community started developing analytical or semi-analytical models to describe the most significant phenomena occurring in this type of contacts [5, 7].

This work aims at combining and analyzing one model involving different aspects in order to accurately describe the dynamic behavior of the contact, together with the aforementioned FE-based approach for the gears bulk compliance. The input for the contact model is the non-linear contact penetration $\delta = -\phi_{EHL}$, which is defined as the distance between the undeformed surfaces of the two bodies along a common normal direction (with the negative sign if the body volumes do not penetrate each other). As described in [8], the penetration can be written as:

$$\delta = -\phi_{EHL} = \delta_{WB} - h_c, \tag{1}$$

where δ_{WB} is the deformation of the solids and h_c is the central fluid film thickness. Due to the similarity between the pressure distribution in EHL contacts and in Hertzian ones [9], we assume that δ_{WB} is approximated by the formulation developed by Weber and Banascheck [10] for dry contacts, while h_c is determined by the model proposed by Moes [11] for steady-state conditions assuming low frequency dynamics. The normal damping of the lubricant is accounted for by the formula proposed by Wiegert et al. [12], while the damping of the solids is neglected since its normal damping is orders of magnitude smaller than the viscous damping of the lubricant. The contact problem is then written as a set of two equations where the normal contact force and the central fluid film thickness are the unknowns. The solution can be computed by any Newton-like method for which a semi-analytic formulation of the Jacobian matrix is given.

Finally, the simulation results employing the contact model together with the gear body linear compliance are presented by means of the dynamic transmission error (DTE) and the time dependent damping coefficient curves during the gears meshing for different operating conditions. The results carried out by the simulations are then compared against experimental test data acquired on a power-recirculation test-rig assessing the accuracy of the modeling technique [13]. The DTE error curves are compared both in terms of shape as well as in terms of their spectrum.

2 Gear meshing modeling

The modeling technique proposed in this work aims at the simulation of an entire transmission, focusing on the development of a strategy for system-level analysis. For this reason this paper adopts a general-purpose multibody (MB) formulation which allows for a good model accuracy and complexity while allowing for a reasonable computation time. This research work focuses on the description of the stiffness and the damping characteristics of a gear pair while the solution of the MB system is computed using the Siemens multibody solver "Motion" available in Virtual.Lab and Simcenter 3D.

When two gears are engaging, the meshing conditions vary during the meshing cycle: in particular the number of teeth pairs in contact, as well as the meshing conditions such as local relative motion of the contacting surfaces, their local curvature and the transmitted load are subject to variations. By exploiting the intrinsic geometric properties of involute gear flanks it is possible to efficiently account for microgeometry modifications, and translational and rotational misalignment. The contact stiffness is non-linear with respect to the load due to the effects of the lubricant and solids in the contact area and increases with the load. Following Andersson and Vedmar [14], the tooth pair compliance is divided in two type of contributions: a local compliance describing the deformation close to the contact area and a bulk compliance describing the contribution due to the deformation far away from the contact region. Figure 1 shows the stiffness decomposition. The meshing of two gears can, in general, be modeled as a variable spring-damper in parallel. This spring-damper (upper Figure 1) can be split in three serial contributions: two linear springs modeling the bulk compliance of the gears and a nonlinear spring-damper to model the full EHL contact, including the lubricant film and local Hertzian deformation of the surfaces. In this case, the damping of the gears body is considered negligible with respect to the viscous damping of the contact.

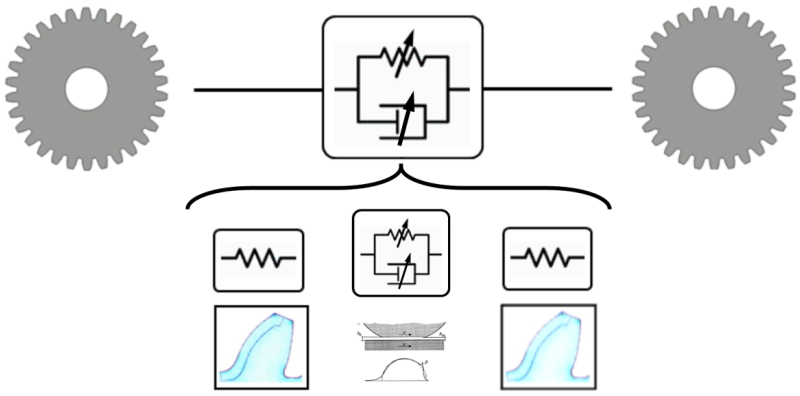

Fig. 1: Tooth pair stiffness and damping decomposition.

Figure 2 shows graphically, the physical meaning of penetration in a tooth pair. The external load in on the meshing gears, is transferred by the lubricant film in between the contacting teeth, and the corresponding pressure-build up is responsible for the local flattening of the surfaces and the bending of the teeth, avoiding as such an unphysical penetration of both gears. The architecture of the MB solver is such that the spatial position and velocity of the two gears is given as input and the corresponding contact force is computed as output. The given penetration is overcome by the local and global deformation of the gears and depends on the stiffness and damping distribution.

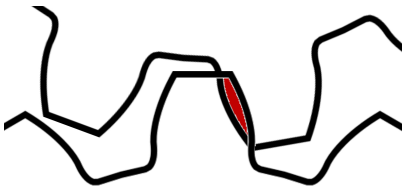

Fig. 2: Penetration in a tooth pair (magnified for visualization).

3 The transient EHL model

As the gears are meshing, the contact conditions, in terms of local geometry, speed, and force, vary over time. This variation causes the fluid film thickness to change continuosly. In this research work, the transient behavior of the lubricated contact is described following the approach of Wiegert et al. [12] who applies a Kelvin-Voigt model in which the spring represents the quasi-static contact stiffness and the damper (placed in parallel) the time-dependent viscous squeeze damping. In order to account for eventual misalignment between the teeth profile or lead modifications, each tooth is divided in a predefined number of slices. Due to symmetries in the assumptions of the contact model, the force has to be applied in the slice center. The latter is chosen on the contact line in correspondence of the mean plane of the slice perpendicular to the contact line. The contact model assumes infinite contact length, neglecting side leakage and boundary effects, which remains compatible with the slicing technique because the slice length is much larger than the characteristic size of the contact.

3.1 Lubricated film thickness in EHL

The steady-state behavior of the EHL contact is in general influenced by the operating conditions, by the properties of the oil and of the solid material and by the local contact geometry. In general, the central fluid film thickness h_c is obtained from equilibrium between the fluid pressure force and the normal load F_{SS} and it is a function of the

parameters representing the above-mentioned characteristics, hence:

$$h_c = f(F_{SS}, R_{eq}, \eta_0, \alpha_{Barus}, u_s, E_{eq}), \tag{2}$$

where R_{eq} represent the reduced radius of curvature of the surfaces, η_0 is the dynamic viscosity of the lubricant, α_{Barus} is the piezo-viscosity coefficient used in Barus [15] formula, u_s is the sum of the speed of the surfaces along the direction perpendicular to the contact direction and E_{eq} represents the reduced Young Modulus. R_{eq} and E_{eq} are calculated as follows:

$$R_{eq} = \left(\frac{1}{R_1} + \frac{1}{R_2}\right)^{-1}, \tag{3}$$

$$E_{eq} = 2\left(\frac{1-\nu_1^2}{E_1} + \frac{1-\nu_2^2}{E_2}\right)^{-1}, \tag{4}$$

where R_1, R_2 are the local radii of curvature of the surfaces in contact, E_1 and E_2 are their Young modulus, ν_1 and ν_2 their Poisson ratios.

Based on the Reynolds equation, Moes [11] made an accurate function fit to predict the central film thickness for a line contact:

$$h_c \;=\; \left[\left(H_{RI}^{7/3} + H_{EI}^{7/3}\right)^{3/7\,s} + \left(H_{RP}^{-7/2} + H_{EP}^{-7/2}\right)^{-2/7\,s}\right]^{s^{-1}} \; U^{-1/2}\, R_{eq} = f(F_{SS}), \tag{5}$$

where $U = \eta_0\, u_s/(R_{eq}\, E_{eq})$ is the dimensionless velocity parameter and s is an auxiliary variable defined as:

$$s \;=\; \frac{1}{5}\left(7 + 8\,\exp\left(-2\,H_{EI}/H_{RI}\right)\right), \tag{6}$$

in which the four basic asymptotes relevant in EHL are shown in Eq. 7 and they are described as function of the dimensionless lubricant (L) and load (M) parameter. As described in [11], the load parameter M is a function of the load exerting on the slice F_{SS}, η_0, u_s, R_{eq}, E_{eq} and the slice width b, while the lubricant parameter L is a function of the Barus [15] parameter α_{Barus}, E_{eq}, R_{eq}, η_0 and u_s.

$$H_{RI} = 3M^{-1}, \qquad H_{EI} = 2.621M^{-1/5}, \qquad H_{RP} = 1.287L^{2/3}, \qquad H_{EP} = 1.311M^{-1/8}L^{3/4}. \tag{7}$$

In the latter equations the subscripts refer to regimes, respectively RI as rigid-isoviscous, RP as rigid-piezoviscous, EI elastic-isoviscous and EP as elastic-piezoviscous. They represent the asymptotes relevant in EHL where the solids can be either rigid or compliant (respectively Rigid or Elastic) and the lubricant can be considered as isoviscous or piezoviscous.

3.2 Lubricant film damping

In EHL contacts, there are two separate damping contributions: one is caused by the viscous forces in the lubricant being squeezed between the surfaces, the other is related to the capacity of the solid material to dissipate energy. Without losing significant accuracy of the model, the damping of the solid material can be considered as negligible with respect to the viscous damping of the lubricant. This assumption is justified in case of steel gears but it might introduce significant errors for visco-plastic materials (e.g. plastic gears).

The damping force F_D is defined as a function of the derivative with respect to time of the fluid film thickness $\dot{h}_c$. This means that every contact parameter influencing the central fluid film thickness h_c influence the damping force as well. Few models exist in literature to model the contact damping without involving iterative schemes and discretization of the contact area. Here we opt to implement the model proposed by Wiegert et al. [12] which defines the damping force as [12]:

$$F_D = -\frac{6.66}{h_c^{3/2}}\, R_{eq}^{3/2}\, \eta_0\, b\, \dot{h}_c, \tag{8}$$

where b represent the contact length. This simple description of the contact damping force is achieved by assuming an isoviscous lubricant, instead of a piezo-viscous lubricant, and neglecting the surfaces deformation. The range of accuracy of the above mentioned assumptions have been investigated in [12] and the results are assumed to be sufficient for a system-level approach as the one targeted by this research.

3.3 Surface local deformation

Due to the similarity in pressure distribution in case of EHL contacts and dry contacts, the deformation of the solid surfaces under the pressure transmitted by the lubricant can be approximated using any Hertz-based formulation. This work uses the formula developed by Weber and Banaschek [10] which allows for considering a finite depth of the material and gives the possibility to be consistent when combing bulk and local compliances. The formula reads [10]:

$$\delta_{WB} = \frac{2F_{SS}}{\pi E_{eq} b} \log\left(\pi h_{tot}^2\right) - \left[\left(\frac{(1-\nu_1)\nu_1}{E_1} + \frac{(1-\nu_2)\nu_2}{E_2}\right)\frac{F_{SS}}{\pi b}\right] - \frac{2F_{SS}}{\pi E_{eq} b} \log\left(\frac{2F_{SS}R_{eq}}{E_{eq} b}\right), \tag{9}$$

where δ_{WB} represents the deformation of the solid bodies due to the applied load F_{SS} and $h_{tot} = h_1 + h_2$ is the total integration depth.

3.4 Local EHL compliance modeling

Figure 3 shows an EHL contact where the contact of two cylinders is modeled using the reduced radius of curvature and the reduced Young's modulus. The position between the undeformed surfaces can be defined by the parameter ϕ_{EHL} representing the gap which is the negative of the penetration. When the load is applied, the surfaces deform increasing the gap by a quantity δ_{WB} to the central fluid film thickness value h_c.

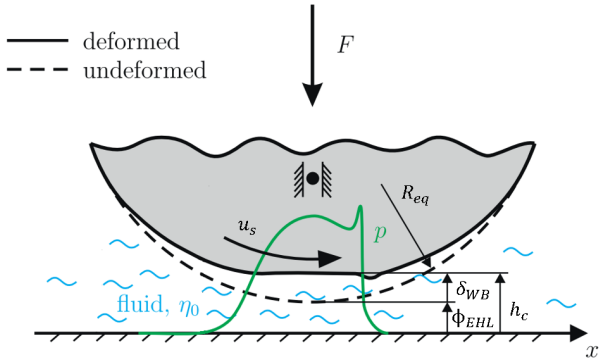

Fig. 3: Elastohydrodynamic contact [12].

There is an equilibrium between the force exerting on the contact F and the steady-state and the damping contribution of the contact:

$$F = F_{SS} + F_D, \tag{10}$$

while according to Figure 3 the fluid film is decomposed as the film thickness of rigid surface and the solid deformation depth:

$$h_c - \delta_{WB} - \phi_{EHL} = 0, \tag{11}$$

Eq. 11 is necessary to relate the gap ϕ_{EHL} with the fluid film thickness. In Eq. 11, ϕ_{EHL} is known a priori and Eq. 5 approximates h_c. The pressure distribution p in the EHL contact is known to be similar to the Hertzian pressure distribution for an equivalent load. Hence, δ_{WB} can be estimated using any Hertz-based load-deflection formula. As above-mentioned, this work uses the formula developed by Weber and Banaschek [10]. Combining Eq. 11 and Eq. 10:

$$g(F,h_c) = h_c - \delta_{WB} = f\left([F - F_D(h_c)]\right) - q\left([F - F_D(h_c)]\right) = \phi_{EHL}, \tag{12}$$

where $F_D = g(h_c, \dot{h}_c)$ according to Eq. 8, $\dot{h}_c$ is approximated by finite differences and $q(F - F_D(h_c))$ represents Weber-Banaschek formula provided in Section 3.3. The local compliance problem with F and h_c representing the unknowns can be written as follows:

$$\mathbf{b}(F,h_c) = \begin{bmatrix} g(F,h_c) \\ f(F,h_c) - h_c \end{bmatrix} = \begin{bmatrix} \phi_{EHL} \\ 0 \end{bmatrix}. \tag{13}$$

4 The bulk compliance of the gears

The bulk compliance of the gears accounts for the tooth bending and shear as well as complex phenomena due to the gear body geometry and coupling between different teeth (e.g. tooth bending due to the bending of the adjacent tooth). The bulk compliance includes global effects that even if they are known to be linear with respect to the applied loads, are generally not representable analytically by any closed-form. In fact the design space for gear bodies and teeth shapes is too wide to be properly captured by a parametric analytical formula. Instead, these types of effects are typically well captured by gears modelled with the finite element (FE) method. To this end an FE model of each gear involved in the contact is created by a semi-automatic procedure [16]. Once the mesh is available, a numerical strategy is adopted to decouple the part of the deformation captured by the underlying FE model and the part captured by the non-linear analytical formulas. This decomposition must be peformed accurately in order to make sure that the local effects are removed and they are not influencing the global compliance. A model order reduction technique is applied in this work, and we refer to [1, 3] for further details. This approach is schematically represented in Figure 4 where the first two images on the right-hand-side represent FE-based calculations while the rightmost image represents the analytical non-linear contact deformation. The FE simulations generate a compliance matrix for each gear. This methodology allows the user to apply this approach to a wide range of cases.

Fig. 4: Computational steps to represent gear total deformation [4].

A special attention is given to the amount and types of coupling terms to be included in the problem solution. With coupling terms we indicate the following effects:

- Slice couplings: When a single axial slice is loaded on a tooth flank, the other slices on the same tooth flank will experience a deformation, effectively contributing to the compliance matrix of the tooth. These terms are always included in the computations.
- Teeth coupling effects: When a single axial slice is loaded on a tooth flank, slices belonging to all the adjacent teeth will experience a deformation effectively contributing to the compliance matrix of the gear pair. In common applications, only a limited amount of teeth is in contact at a certain instant in time so that the amount of teeth coupling terms can be limited, effectively reducing storage and computational time. The user can chose to increase the complexity and accuracy of the simulation by including or excluding these effects.

The coupling terms between slices and more importantly between teeth are a truly unique feature of this method for multibody systems and is an important contribution to the high accuracy of the method. They represent a key factor when it comes to predict the moment when a tooth pair enters in contact and in the overall meshing stiffness evaluation.

4.1 Compliance matrix creation

The creation of the gear compliance matrix involves the computation of a reduction space that is used to condense the information contained in the underlying FE stiffness matrix of the gears. To obtain the reduction space, a procedure similar to [3] is employed which leverages a series of static FE solutions for each potential node in contact node. The reduction space contains only the global deformations the gears. For the majority of the cases,

it is enough to extract deformation patterns for a limited set of FE nodes (e.g. 50-70% of the nodes on the teeth flanks). The reduction space obtained Ψ^i is used to reduce the stiffness matrix of the underlying FE model.

$$K^i_{red} = \Psi^{i^T} K^i_{FE} \Psi^i, \tag{14}$$

where K^i_{FE} is the FE stiffness matrix of gear and K^i_{red} is the reduced stiffness matrix. The inverse of the reduced stiffness matrix is used internally in the multibody solver to create the compliance matrix C^i mapped onto the gear axial slices.

In some circumstances, the amount of vectors to be included in the reduction space can become significant, leading to a large stiffness matrix K^i_{red} [17]. This issue is more common with non-axisymmetric gears with a large number of teeth. On the other hand it is important to notice that due to the rotation of the gears, only a few teeth are actively involved in the contact at a certain moment in time. For this reason, the assembly of the reduced stiffness matrix is performed dynamically during the simulation using only the part of the database related to the part of K^i_{red} that is involved in the contact at a certain moment in time. This procedure is closely related to the static modes switching method proposed in [17]. The contact forces are computed in a quasi-static fashion which keep the numerical procedure smooth and at each time-step the algorithm obtains convergence without spurious oscillations. The update of the compliance database takes place every time that a new tooth pair enters or exits contact or when the amount of teeth potentially in contact changes e.g. due to a center distance variation. In this way an optimally small database is retained and the inverse of the reduced stiffness matrix is updated only when necessary with clear computational benefits.

5 Architecture of the numerical model

After the contact detection is performed and the bulk compliance matrices are built, within a time step the solver calls for the contact force between two gears to be computed. At this point the local compliance and the bulk compliance have to be summarized in a mathematical fashion to calculate the corresponding force exchanged by the meshing gears. The problem can be arranged as a set of non-linear equations as follows:

$$\mathbf{C} \cdot \begin{bmatrix} \mathbf{F}_{1,2} \\ \mathbf{h}_c \end{bmatrix} + \begin{bmatrix} \mathbf{g}(\mathbf{F}_{1,2}, \mathbf{h}_c) \\ \mathbf{f}(\mathbf{F}_{1,2}, \mathbf{h}_c) \end{bmatrix} - \begin{bmatrix} \boldsymbol{\delta}_{1,2} \\ \mathbf{0} \end{bmatrix} = 0, \tag{15}$$

where:

- $\mathbf{F}_{1,2}$ is the vector of the unknown contact forces along the normal direction to the involute profile;
- $\mathbf{h}_c$ is the unknown vector of the fluid film thicknesses for each slice and each tooth pair in contact;
- $\mathbf{g}(\mathbf{F}_{1,2}, \mathbf{h}_c)$ and $\mathbf{f}(\mathbf{F}_{1,2}, \mathbf{h}_c)$ are non-linear functions representing the local EHL contact model. They are function of the unknowns;
- $\boldsymbol{\delta}_{1,2}$ is the vector of instantaneous penetrations on each active slice of the teeth that are in contact at a certain time instant. The penetration vector accounts is corrected for the microgeometry correction of the gear in the normal direction;
- $\mathbf{C}$ is a block diagonal matrix defined as follows:

$$\mathbf{C} = \begin{bmatrix} \mathbf{C}^1 + \mathbf{C}^2 & \mathbf{0} \\ \mathbf{0} & -\mathbf{I} \end{bmatrix}, \tag{16}$$

  where $\mathbf{C}^1$ and $\mathbf{C}^2$ are full matrices that include the FE based compliance for gear 1 and gear 2 and $-I$ represents $\mathbf{h}_c$ from Eq. 13.

It can be noticed that due to the full nature of the C^i matrices, the amount of penetration on each slice is highly dependent on the penetration (and contact forces) acting on all the potentially active slices. In practice the amount and location of the active slices is not known before the solution of Eq. 15. In fact, some slices can enter or exit the contact due to the load on any neighboring slice. The system of equations can be solved employing any Newton based iterative scheme. The following considerations make the suggested approach computationally attractive and scalable from a user point of view:

- The separation between global and contact compliance allows to adopt a relatively coarse mesh (usually 6-12 elements on the profile and 4-12 elements on the width are enough for cylindrical gears) as compared to typical contact mechanics FE meshes where the contact areas have to be highly discretized.
- The slicing approach allows the user to select a number of slices in which the instantaneous axial overlap is divided. A number of slices that is similar in number to the amount of element along the teeth axes is usually suggested.
- Since contact forces are computed including a non-linear local compliance term, the contact stiffness presents the typical stiffening behavior with increasing contact loads.

The implementation of a Newton based scheme requires the Jacobian matrix to be computed with respect to the unknowns $\mathbf{h}_c$ and $\mathbf{F}_{1,2}$. Since the problem can become rather stiff, the Jacobian should be well approximated to assure a convergent iterative scheme. The linear part of Eq. 15 contributes to the Jacobian by the matrix C while for what concerns the local compliance its contribution to the global Jacobian can be computed as follows:

$$\frac{dg(F,h_c)}{dF} = \frac{\partial f}{\partial F_{SS}} \cdot \frac{\partial F_{SS}}{\partial F} - \frac{\partial q}{\partial F_{SS}} \cdot \frac{\partial F_{SS}}{\partial F} = \frac{\partial f}{\partial F_{SS}} - \frac{\partial q}{\partial F_{SS}}, \tag{17}$$

$$\frac{df(F,h_c)}{dF} = \frac{\partial f}{\partial F_{SS}} \cdot \frac{\partial F_{SS}}{\partial F} = \frac{\partial f}{\partial F_{SS}}, \tag{18}$$

$$\frac{dg(F,h_c)}{dh_c} = \frac{\partial f}{\partial F_{SS}} \cdot \frac{\partial F_{SS}}{\partial h_c} - \frac{\partial q}{\partial F_{SS}} \cdot \frac{\partial F_{SS}}{\partial h_c}, \tag{19}$$

$$\frac{df(F,h_c)}{dh_c} = \frac{\partial f}{\partial F_{SS}} \cdot \frac{\partial F_{SS}}{\partial h_c}. \tag{20}$$

Using the formula (17)-(20) only three partial derivatives have to be computed. In particular:

- $\frac{\partial f}{\partial F_{SS}}$ can be computed analytically or numerically;
- $\frac{\partial q}{\partial F_{SS}}$ can be computed analytically;
- $\frac{\partial F_{SS}}{\partial h_c}$ can be computed either numerically or analytically.

Once all the contributions of the Jacobian are computed, the Jacobian matrix is defined by summing the necessary partial contributions and the matrix C.

6 Validation

The procedure presented in this paper is implemented in the Siemens Virtual.Lab Motion solver and then validated against experimental test data. The goal of the validation is to assess the accuracy of the contact model for system-level analysis with respect to experimental test data. The experimental campaign was carried out thanks to an in-house precision gear test-rig [13] jointly developed by Siemens PLM Software, KU Leuven and the University of Calabria.

Experimental test data and simulations are compared by means of TE (transmission error) [18] representing a KPI (key performance indicator) largely adopted to evaluate the NVH performances of a geared transmission. For what concerns the contact modeling validation, by comparing the test data against simulations we can assess the validity of the proposed model for system-level analysis despite the experimental test data cannot give specific information regarding the EHL contact behavior.

6.1 The experimental test set up

The test-rig (see Figure 5) has been designed and manufactured to assess typical gear-related physical quantities in static and dynamic conditions, under imposed conditions of misalignment and shaft compliances. The setup is composed of two main parts: the test side and the reaction side. These parts are dynamically separated from each other by using flexible couplings. Designed in a power-recirculating arrangement, it allows a small electric motor to spin the shafts. This simplifies the application of smooth speed and constant torque preloads and facilitates the measurement of rotational and lateral vibrations in the system. The raw data obtained from the experiment is then post-processed to obtain frequency and order domain results.

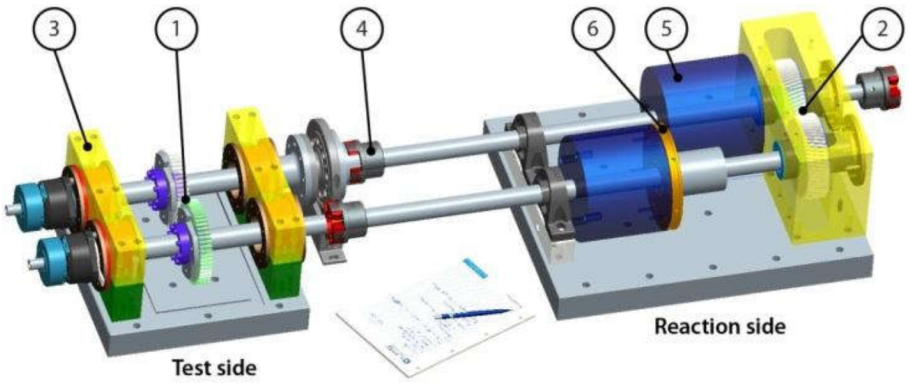

Fig. 5: Test-rig three-dimensional representation. 1. Test gears; 2. Reaction gears; 3. Bearings support; 4. Flexible couplings; 5. Flywheel; 6. Clutch flange for preload.

The gears used in the test campaign were manufactured with tight tolerances and measured tooth by tooth in the profile and lead directions. Tooth surfaces have been hardened and precision ground to ISO quality 3 (equivalent to AGMA 15). The gears are designed in such a way that the signal to noise ratio of the TE is emphasized, due to higher tooth compliance. The test side of the setup is instrumented as Figure 6 shows.

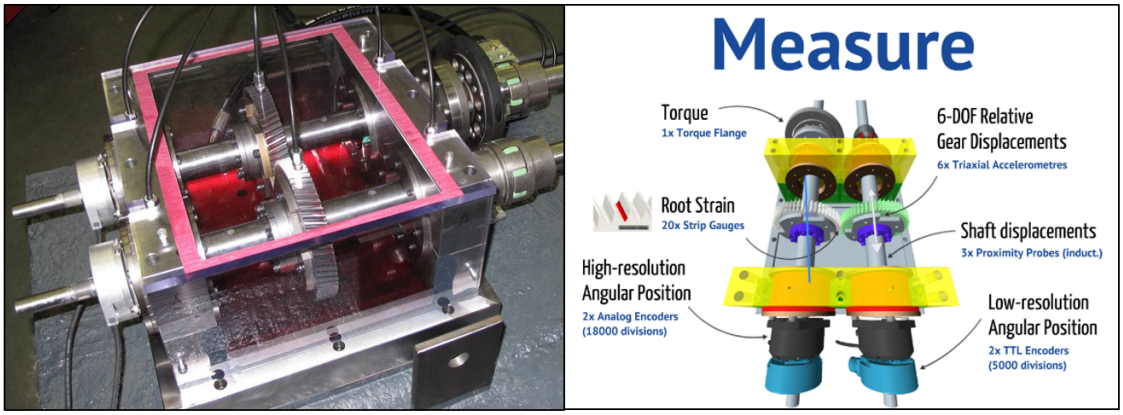

Fig. 6: Test side of the test-rig and its instrumentation.

This validation work was performed using a gear pair configuration involving one solid gear (P2) and one with axisymmetric lightweight design (SUC) as shown in Figure 7. The lubricant used to perform the test campaign is Euroil ATF 6700 which has the viscosity reported in Table 1 while the Barus coefficient has been estimated. The tested gears and the lubricant used on the test-rig have the geometrical specifications listed in Table 1. Each test is performed at a constant torque and the gears rotating with a constant speed. While only one level of torque is used (150 Nm), two different rotational speeds are given to the setup, respectively: 750 rpm and 1500 rpm in order to not excite the resonances of other components with the tooth passing orders. For further investigations see [19].

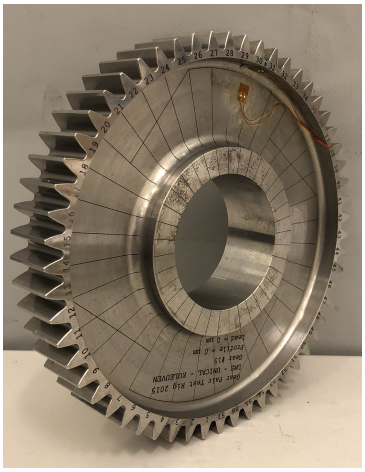

(a) *SUC gear.*

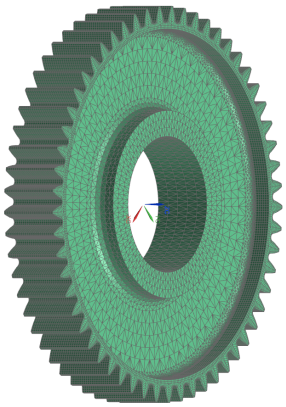

(b) *FEM of SUC gear.*

Fig. 7: Tested gear with lightweight design (SUC).

	Parameters	**Units**	**Gear-set SUC-P2**
Gears	Driving gear tooth number	$[-]$	57
	Driven gear tooth number	$[-]$	57
	Helix angle	[deg]	0
	Pressure angle	[deg]	20
	Module	[mm]	2.6
	Face width	[mm]	23
	Center distance	[mm]	150
	Micro-modifications	$[\mu$m]	P2: 10 (profile crowning)
Lubricant	Nominal viscosity @ 40°C	[Pa s]	0.025
	Barus coefficient [15]	$[\text{Pa}^{-1}]$	$2.5 \cdot 10^{-8}$

Tab. 1: Gear SUC-P2 and oil specifications.

6.2 The multibody model

An MB model of the test-rig was built in Siemens Virtual.Lab Motion as Figure 8 shows. The MB model of the test-rig has the following features:

1. SUC-P2 gear pair;
2. Bushing elements with 5-by-5 stiffness and damping matrices representing the self-aligning double-row cylindrical roller bearings;
3. Bushing elements representing the flexible couplings connecting the test side with the flywheels;
4. Relative position bracket joint to introduce the preload in the system.

The gear response is calculated by the above-described methodology, accounting for the compliance of the gears body and the effects of the lubricant in the contact area. A torque and a rotational damping is given to simulate the motor input. Once the shafts are rotating at the target speed, the torque due to the damping balances the input torque and the system keeps rotating at the target speed while allowing for small fluctuations of the rotational speed. The MB simulations are run using the simulation parameters in Table 2. The number of slices was chosen in order to have a fast computation while maintaining a good level of accuracy. The friction coefficient cannot be estimated using the proposed modeling technique.

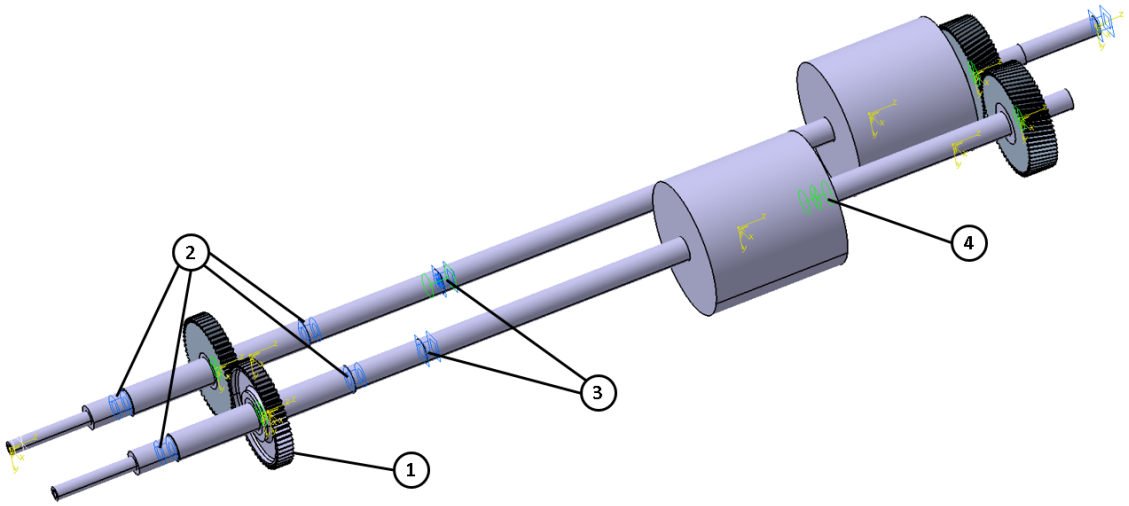

Fig. 8: The MB model of the test-rig.

	Parameters	Units	Value
Test Gears	Number of slices	[−]	3
	Bulk compliance	[−]	FE Preprocessor
Reaction Gears	Number of slices	[−]	2
	Bulk compliance	[−]	FE Preprocessor
Bearings	Radial stiffness	[N/m]	$3 \cdot 10^8$
	Axial stiffness	[N/m]	$3.68 \cdot 10^7$
	Conical stiffness	[Nm/rad]	1
	Radial damping	[kg/s]	5
	Axial damping	[kg/s]	5
	Conical damping	[kgm^2/(s rad)]	1
Couplings	Torsional stiffness	[N m/rad]	5740
	Torsional damping	[kgm^2/(s rad)]	5
Actuation	Torque	[N m]	500
	Damping (750 rpm)	[Nm/rpm]	0.667
	Damping (1500 rpm)	[Nm/rpm]	0.334
Simulation	Simulation Time	[s]	1.3
	Time Step	[s]	10^{-5}

Tab. 2: Simulation parameters.

6.3 Comparison between simulations and experimental test data

The comparison between simulation and experimental test data is done by means of TE curves in angle domain (Figure 9) and the spectrum in order domain (Figure 10). The orders related to the tooth passing frequency (57^{th}, 114^{th}, 171^{st} etc.) are easily recognizable and their positions in the spectrum do not depend on the speed of the shaft. The TE raw data are filtered in order to remove the low frequency oscillations caused by the geometrical imperfections of the system (e.g. shafts straightness tolerance). These phenomena usually have a frequency below the $30^{th} - 40^{th}$ order so they can be easily removed without compromising the global accuracy of the signal.

Figure 9 shows a comparison between the TE acquired on the test-rig and the TE simulated using the model proposed in this paper. As mentioned earlier in this paper, two cases are studied, respectively 750 rpm with 150 Nm preload in Figure 9a and 1500 rpm with 150 Nm preload in Figure 9b. From Figure 9 is clear how the global shape of the TE is correctly foreseen. Preliminary tests using more accurate Flexible MB model of the test rig (future

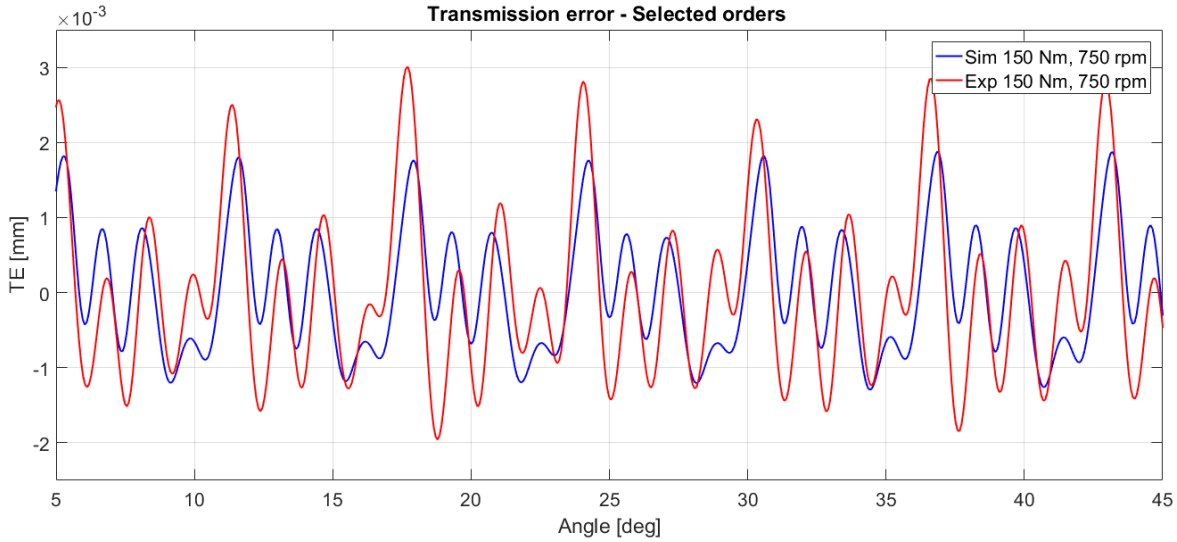

(a) *TE in angle domain at 750 rpm and 150 Nm.*

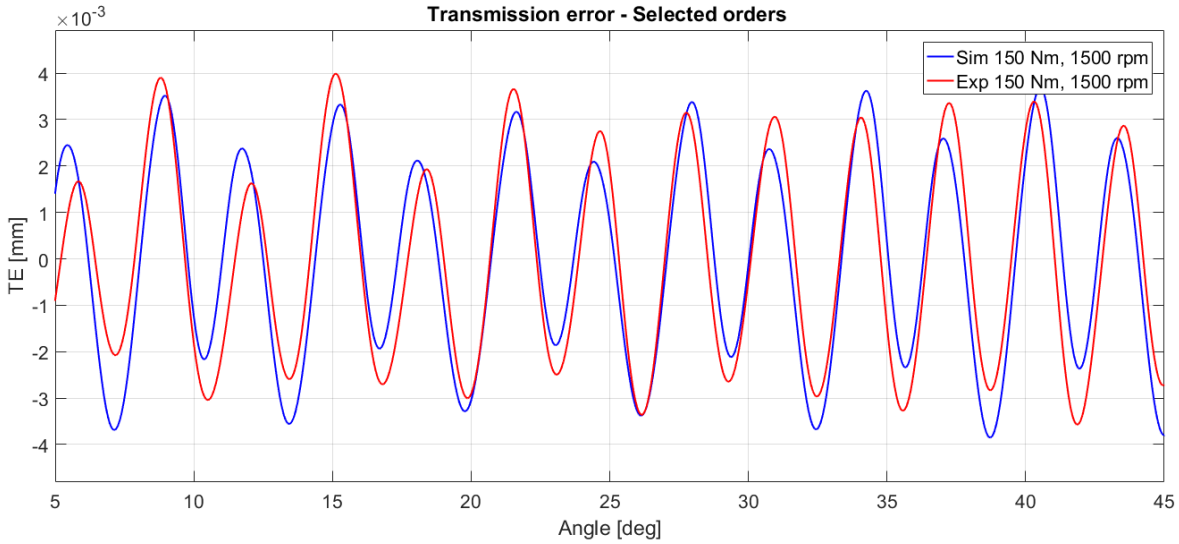

(b) *TE in angle domain at 1500 rpm and 150 Nm.*

Fig. 9: Comparison between experimental test data and simulation data in terms of TE.

work), have shown that the discrepancy between the curves is caused by the limitations of the current rigid MB model.

In order to quantify the accuracy of the numerical model with respect to the experimental test data, the spectra in order domain of the TE for both cases are compared in Figure 10. As spectrum the *Power Spectral Density* (PSD) [20] is employed in order to normalize the signal w.r.t the data acquisition parameter.

Figure 10 shows how the dominant orders are well approximated by the model, while less relevant orders have less accuracy. Dominant orders are the ones that contributes the most in the TE (i.e. 57^{th}, 114^{th} and 228^{th} for 750 rpm and 57^{th}, 114^{th} for 1500 rpm). The lowe accuracy of less relevant orders can be addressed to the rigid model of the test-rig where no flexibility of the bodies (except for the gears) is accounted for. As described in [19] most of the mode shapes of the test-rig involve the flexibility of the shafts which cannot be represented by this model. Moreover when comparing the orders, in case of experimental test data the orders that are not related to the tooth passing frequency are higher with respect to the simulation data. This is due to the noises of the signal when acquiring experimental data of a physical system.

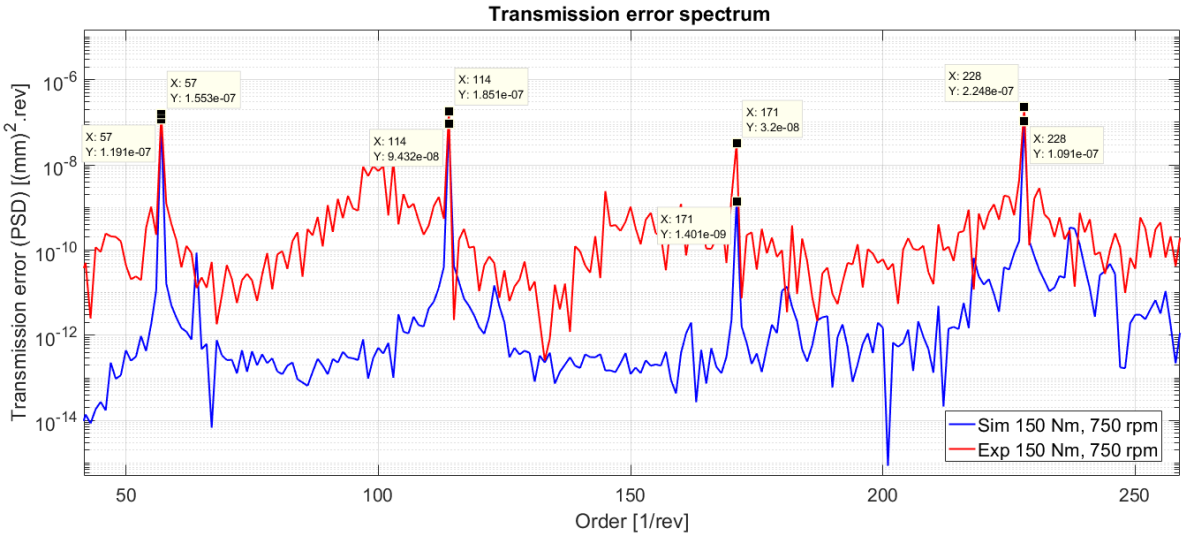

(a) *TE spectrum at 750 rpm and 150 Nm.*

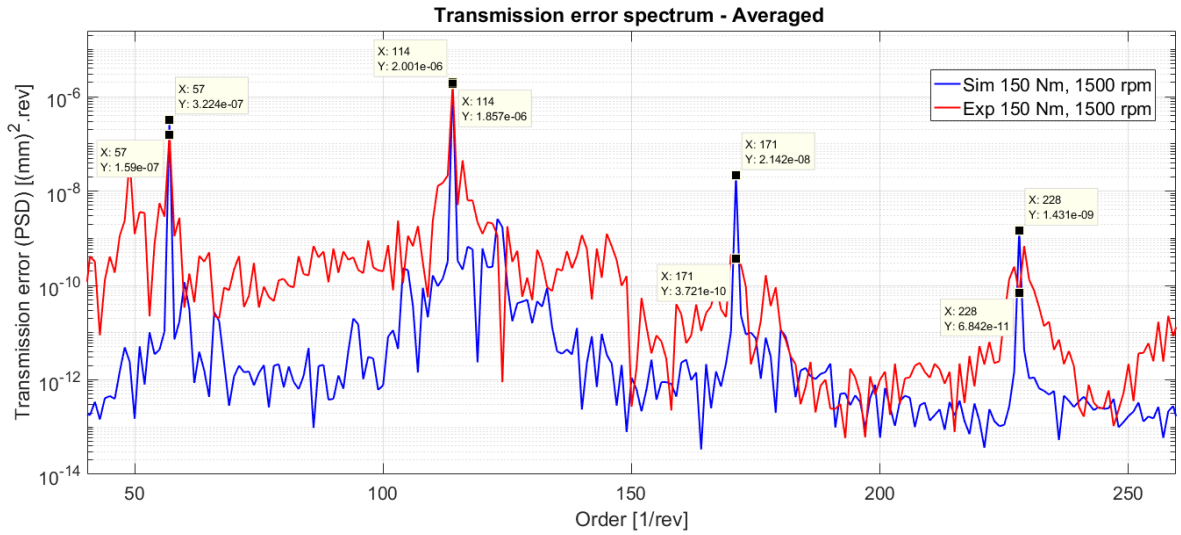

(b) *TE spectrum at 1500 rpm and 150 Nm.*

Fig. 10: Comparison between experimental test data and simulation data in terms of TE spectrum.

6.4 The contact damping coefficient

In this section, the damping coefficient of the contact is showed and analyzed by means of its mean value and its variance throughout the meshing cycle. According to Eq. 8 the damping coefficient is defined as:

$$C_D = -\frac{6.66}{h_c^{3/2}} R_{eq}^{3/2} \eta_0 \, b. \tag{21}$$

During a meshing cycle the contact conditions (e.g. relative speed of the surfaces, radii of curvature etc.) vary, causing the damping coefficient to change as well. Table 3 lists the mean damping values D_m for each case study. The damping coefficient is calculated summing the contribution in damping of all the slices and flanks in contact. It is clear how the rotational speed of the gears has an important influence on the damping coefficient. This is due to the influence the surfaces speed has on the fluid film thickness. In particular, when the the sum of the speed of the surfaces increases, maintaining the same load, h_c increases, hence according with Eq. 21 the damping coefficient decreases.

	750 rpm	1500 rpm
D_m [Ns/m]	-124.3	-78.4

Tab. 3: Mean value of the damping coefficient of the contact.

Figure 11 instead shows the damping coefficient over the rotation angle of the gears. Two oscillations with different amplitude can be recognized:

- Modulation with high amplitude: it is caused by the change in number of teeth pair in contact and it gives the main contribution to the peak-to-peak value of the curve;
- Modulation with lower amplitude: it is caused by different contact conditions such as surfaces speed, radii of curvature etc. it is more evident where the damping coefficient is at its minimum absolute value. It is characterized by lower amplitude since the change in contact conditions is less relevant than the change in number of tooth pairs in contact.

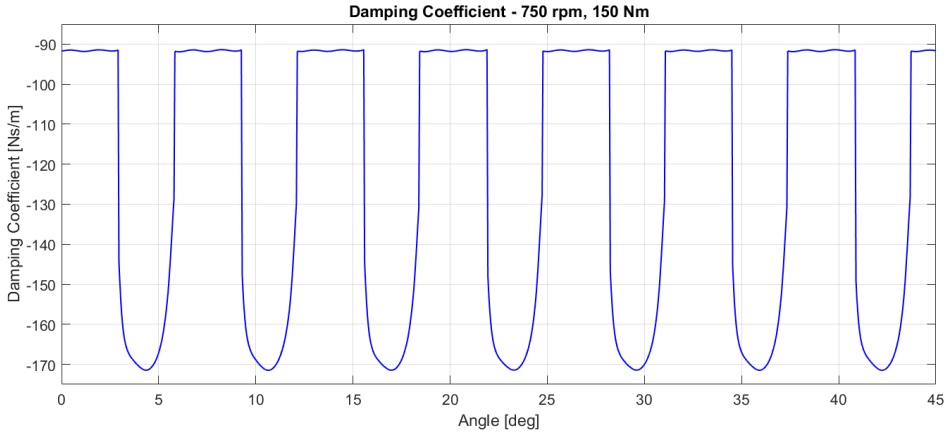

(a) *Damping coefficient at 750 rpm and 150 Nm*

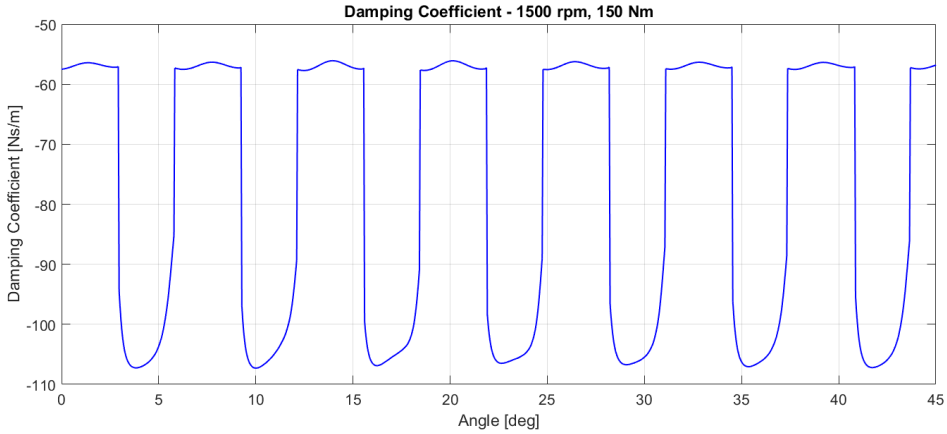

(b) *Damping coefficient at 1500 rpm and 150 Nm*

Fig. 11: Contact damping coefficient over angle.

By Table 3 it is clear how a constant damping coefficient would not be suitable for a simulation in which the rotational speed of the gears vary. While Figure 11 underlines the importance of having a model for the damping in order to correctly estimate the fluctuation of the damping coefficient during the meshing cycle.

6.5 Comparison against the dry contact model

To understand the advantages of the contact model proposed in this paper is interesting to compare the results obtained with the EHL model against the Hertz-based contact model [16] both using the FE Preprocessor to model the bulk compliance. This comparison is shown in order to underline the relevance of the added complexity to have more accurate simulation with respect to the already established Herz-based contact model. The dry contact model employs the formula of Weber and Banascheck [10]. In order to apply such a model, the user must input a damping value for the contact since the model is not capable of estimating it. Guessing a damping coefficient can be relatively straight forward in case of quasi-static simulations (low rpm regime) while it can turn out to be more complicated with a transient system due to sensitivity of the system response with the contact damping. When dry contact is considered, the damping coefficient remains constant throughout the meshing cycle.

In order to be consistent, the damping coefficient for the dry model is considered equal to the mean value of the one calculated with the EHL model (see Table 3). Moreover, the simulations with the EHL and dry contact model uses the same parameters listed in Table 2. Figure 12 shows the simulations results including the experimental test data for both 1500 rpm and 750 rpm.

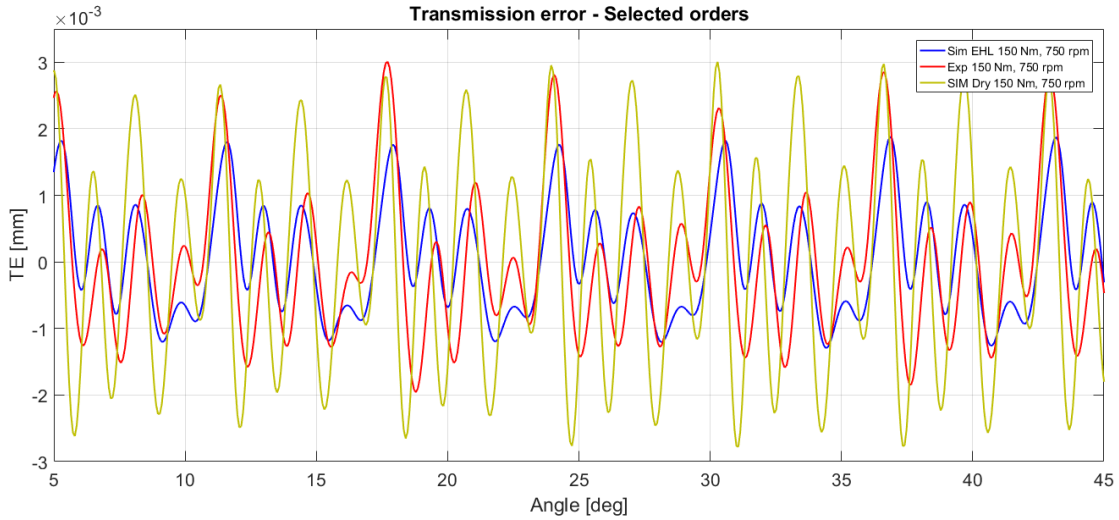

(a) *TE in angle domain at 750 rpm and 150 Nm*

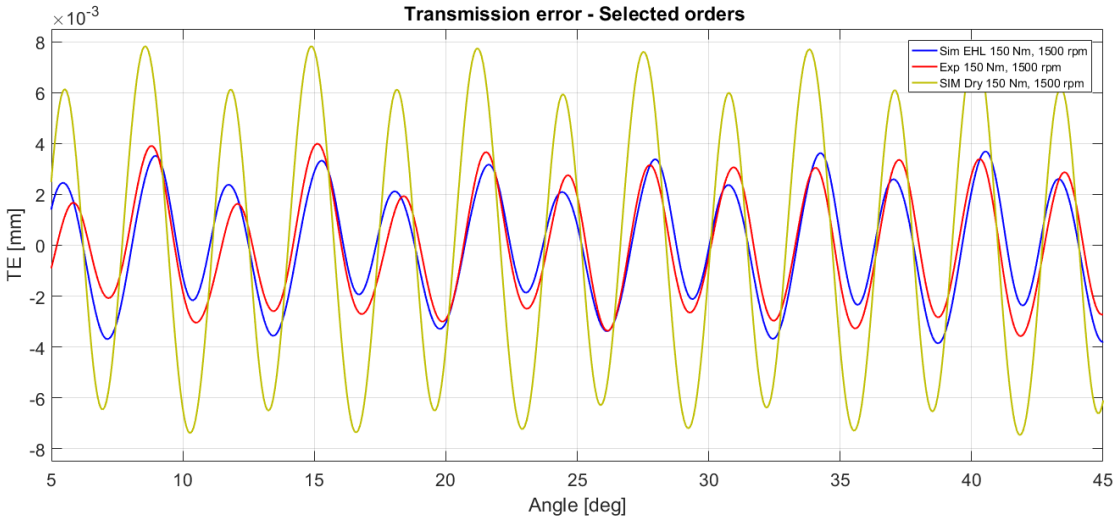

(b) *TE in angle domain at 1500 rpm and 150 Nm*

Fig. 12: TE comparison between EHL and dry contact model and experimental test data.

From Figure 12 is clear how the EHL model is capable of fitting the experimental test data better than the dry contact model. This can be addresses to two main factors:

- As pointed out by Figure 11, the damping coefficient is not constant and its value can span in a wide range during a meshing cycle. By considering a constant damping coefficient the damping force is overestimated or underestimated depending on the contact conditions which have a negative impact on the accuracy of the simulation.
- Due to the fluid film thickness, the gears are, in general, in a different configuration with respect to when using the dry contact model. This can lead to a different results when performing the contact detection (e.g. a teeth pair can have a delayed engaging moment if the adjacent teeth pair is considered as working in lubricated conditions).

Of course the level of accuracy gained with the analytical EHL contact model is payed back with a time required for the simulation to compute that is $1.5 - 2$ times greater than when using the dry contact model.

7 Conclusions and future developments

The preliminary results showed in this work demonstrate that the model is a significant improvement to current Hertz-based models for system-level MB analysis of mechanical transmissions, and proved its importance especially in cases where the rotational speed of the gears spans over a wide range which lead to a damping coefficient that can vary by orders of magnitude. The validation showed in this paper will be further extended with more detailed analysis. Two different paths are currently in development: in line with the validation showed in this paper the MB model will be improved to introduce the test shafts flexibility by means of flexible MB modeling in order to correctly simulate more operative conditions, in addition to this, a parallel validation work is currently ongoing to evaluate the accuracy of the contact model itself, in particular a FSI (Fluid Structure Interaction) model is on development using the commercial software Star-CCM+ from Siemens CD Adapco in order to have a reference to quantify the level of accuracy of the contact model in different contact conditions.

Acknowledgements

The authors gratefully acknowledge VLAIO (Agency for Innovation by Science and Technology in Flanders) for the financial support through the ECOPowertrain project (Ref nr 150394) and through the Baekeland Mandate ref nr 160228 which funds the research of Leoluca Scurria.

References

[1] L. Vedmar, *On the design of external involute helical gears*. Transactions of Machine Elements Division, Lund Technical University, Lund, 1981.

[2] T. Tamarozzi, G. H. Heirman, and W. Desmet, "An on-line time dependent parametric model order reduction scheme with focus on dynamic stress recovery," *Computer Methods in Applied Mechanics and Engineering*, vol. 268, pp. 336–358, 2014.

[3] N. Cappellini, T. Tamarozzi, B. Blockmans, J. Fiszer, F. Cosco, and W. Desmet, "Semi-analytic contact technique in a non-linear parametric model order reduction method for gear simulations," *Meccanica*, pp. 1–27, 2017.

[4] N. Cappellini, B. Blockmans, J. Fiszer, T. Tamarozzi, F. Cosco, and W. Desmet, "Reduced-order modelling of multibody contact problems: A novel semi-analytic method," in *13th International Conference on Multibody Systems, Nonlinear Dynamics and Control*, American Society of Mechanical Engineers, 2017.

[5] P. Fietkau and B. Bertsche, "Efficient simulation of gear contacts including transient elastohydrodynamic effects," *Journal of Tribology*, vol. 135, no. 3, p. 031502, 2013.

[6] A. Hajishafiee, *Finite-volume CFD modelling of fluid-solid interaction in EHL contacts*. PhD thesis, Imperial College London, 2013.

[7] S. Li and A. Kahraman, "A spur gear mesh interface damping model based on elastohydrodynamic contact behaviour," *International Journal of Powertrains*, vol. 1, no. 1, pp. 4–21, 2011.

[8] L. Scurria, J. Fiszer, T. Tamarozzi, P. Jiranek, and W. Desmet, "An advanced modeling technique for rolling element bearings in elastohydrodynamic field," *Rolling contact Mechanics for Multibody System Dynamics*, 2017.

[9] R. Gohar, *Elastohydrodynamics*. World Scientific, 1988.

[10] C. Weber and K. Banaschek, "Formänderung und Profilrücknahme bei Gerad-und Schrägverzahnten Antriebstechnik," *Vieweg, Braunschweig*, vol. 11, 1953.

[11] H. Moes, "Optimum similarity analysis with applications to elastohydrodynamic lubrication," *Wear*, vol. 159, no. 1, pp. 57–66, 1992.

[12] B. Wiegert, H. Hetzler, and W. Seemann, "A simplified elastohydrodynamic contact model capturing the nonlinear vibration behaviour," *Tribology International*, vol. 59, pp. 79–89, 2013.

[13] A. Palermo, A. Toso, G. Heirman, R. Cerdá, M. Gulinelli, D. Mundo, and W. Desmet, "Structural coupling and non-linear effects in the experimental modal analysis of a precision gear test rig," in *International Gear Conference*, vol. 2014, pp. 1049–1059, 2014.

[14] A. Andersson and L. Vedmar, "A dynamic model to determine vibrations in involute helical gears," *Journal of Sound and Vibration*, vol. 260, no. 2, pp. 195–212, 2003.

[15] C. Barus, "Isothermals, isopiestics and isometrics relative to viscosity," *American Journal of Science*, no. 266, pp. 87–96, 1893.

[16] "Siemens PLM Software: Boosting Productivity in Gearbox Design - white paper - last accessed on 17/4/2019," tech. rep., "https://www.plm.automation.siemens.com/en/products/lms/virtual-lab/motion/dynamic.shtml#lightview%26url=/en_us/Images/Siemens-PLM-Boosting-Productivity-in-Gearbox-Engineering-wp-65217-A20_tcm1023-259449.pdf%26title=Boosting%20Productivity%20in%20Gearbox%20Engineering%26description=%26docType=pdf".

[17] G. H. Heirman, T. Tamarozzi, and W. Desmet, "Static modes switching for more efficient flexible multibody simulation," *International Journal for Numerical Methods in Engineering*, vol. 87, no. 11, pp. 1025–1045, 2011.

[18] A. Palermo, L. Britte, K. Janssens, D. Mundo, and W. Desmet, "The measurement of gear transmission error as an NVH indicator: Theoretical discussion and industrial application via low-cost digital encoders to an all-electric vehicle gearbox," *Mechanical Systems and Signal Processing*, vol. 110, pp. 368–389, 2018.

[19] A. Dabizzi, G. Heirman, A. Palermo, S. Manzato, S. Shweiki, and A. Toso, "Multibody modeling of a high precision gear test rig and correlation to experiments," in *Proceedings of ISMA2016*, pp. 1371–1382, 2016.

[20] A. Brandt, *Noise and Vibration Analysis: Signal Analysis and Experimental Procedures*. John Wiley & Sons, 2011.